Highlights

Energy Preserving High Order Mimetic Methods For Hamiltonian Equations

Anand Srinivasan, José E. Castillo

- High order mimetic operators
- Mimetic difference methods
- Energy preserving composition schemes
- Linear and non-linear Hamiltonians

Energy Preserving High Order Mimetic Methods For Hamiltonian Equations

Anand Srinivasan a,* , José E. Castillo b

ARTICLE INFO

Keywords: mimetic high order composition schemes Hamiltonian energy preserving

ABSTRACT

Hamiltonian equations possess a Hamiltonian function that governs the conserved physical property for the system. Obtaining a discretization scheme that satisfies the intrinsic geometric properties of its continuum problem is often a challenge. Spatial schemes that discretely mimic a conservation law are known to result in accurate discretizations of partial differential equations. The mimetic methods considered in this paper for spatial discretization are based on the work of Castillo & coauthors. These methods produce high order mimetic operators which, by construction, result in a discrete equivalent to a conservation law. These operators work on staggered spatial grids and produce even orders of accuracy at the boundaries and interiors, while avoiding the use of ghost nodes. The high order mimetic operators D and G are discrete approximations of their continuum counterpart vector calculus identities of divergence and gradient. The resulting discretizations are therefore said to mimic the underlying physics. The preservation of the spatio-temporal energy evolution requires a corresponding time integration scheme that is structure preserving, such as the staggered leapfrog scheme. The traditional leapfrog scheme, however, is limited to second order accuracy. In this work, we study the high order composition temporal methods with the mimetic operators to investigate the energy preserving aspects of Hamiltonian systems. Fourth and sixth order spatio-temporal energy preserving schemes are presented for both linear and non-linear Hamiltonian systems. The novelty of this work includes the validation of a sixth order mimetic energy preserving numerical scheme for non-linear Hamiltonian systems. Numerical examples that illustrate our findings are also presented in this work.

1. Introduction

Hamiltonian systems are a class of partial differential equations (PDEs) used prevalently in engineering and sciences [?], such as the shallow water equations [?], the wave equation [?] and Maxwell's equations [?]. A defining feature of Hamiltonian systems is the Hamiltonian function, which is a measure of the energy of the physical system modeled by the PDE. Numerical schemes that discretely preserve this energy evolution are a necessity for accurate long-term spatio-temporal solutions of Hamiltonian PDEs.

Obtaining such energy preserving numerical solutions with optimal computational cost is often a challenge [?]. Broadly speaking, the scheme ought to satisfy certain requirements for both the spatial and temporal discretizations. Spatial discretization schemes that mimic a conservation law are known to result in energy-stable discretizations [?]. The divergence theorem states that the integral of the divergence of the flux over a volume equals the integral of the flux across the surface. Discrete spatial operators that mimic this continuum property lead to stable, energy-preserving and positivity-preserving spatial discretizations [?]. In a one-dimensional framework, the continuum version of the extended Gauss divergence theorem becomes integration by parts which the Castillo-Grone mimetic operators satisfy

[?]. The classical quadrature rules often fail to discretely mimic the quadrature over a volume to produce a quadrature over the surface [?] while the Corbino-Castillo mimetic quadratures satisfy the divergence theorem [?].

The mimetic methods developed by Castillo & Grone [?] result in high order discrete equivalents for the vector calculus identities of divergence and gradient. The underlying idea behind the Castillo-Grone methods lies in the fact that the discrete operators are developed by mirroring the properties of a fundamental conservation law. As a result, the mimetic operators mimic the desirable properties of their continuum ones. The resulting operators have been shown to possess the desired spatial orders of convergence [?] while operating on staggered grids. Moreover, the order of spatial accuracy is uniform (and even order; i.e., orders 2, 4, 6 and higher) at the boundaries and interiors of the grid [?], and is achieved while avoiding the use of ghost nodes (which are non-physical cells outside of the physical domain).

The Castillo-Grone methodology has free-parameters in the derivation of the mimetic operators. The upgraded methodology of Corbino-Castillo [?] retains the same mimetic character for the high order mimetic operators while avoiding the use of free-parameters. Moreover, the Corbino-Castillo operators possess optimal bandwidth for the div and grad matrices. In this work, the Corbino-Castillo operators are used as the basis for the spatial discretization.

Spatio-temporal PDEs are numerically solved using the semi-discrete approach, where the domain is discretized in space first, followed by integration in time. The Leapfrog scheme (also referred to as the Verlet method [?]) is a

^aComputational Science Research Center, San Diego State University, San Diego, 92182, CA, USA

^bComputational Science Research Center, San Diego State University, San Diego, 92182, CA, USA

^{*}Corresponding author

[🔊] asrinivasan0709@sdsu.edu (A. Srinivasan); jcastillo@sdsu.edu J.E. Castillo)

ORCID(s): 0009-0005-4231-925X (A. Srinivasan); 0000-0001-9215-1559 (J.E. Castillo)

staggered temporal scheme that possesses symplectic qualities [?]. However, it only possesses second order temporal accuracy. Symplectic integrators such as the Forest-Ruth algorithms [? ?] are limited to fourth order temporal accuracy, and are also not staggered in time. Although other symplectic integrators exist in the literature for Hamiltonian systems, these are more often implicit integration schemes [?] that add a burden to the computational cost. The relaxation Runge Kutta schemes [?] that provide a viable option to converting the traditional Runge Kutta methods into an energy conserving scheme was investigated with the mimetic operators in [?]. However, the computational effort in calculating the relaxation parameter for each step of integration imposes a computational overhead [?]. The staggered temporal schemes of Williams [??] was investigated in [?] using the mimetic spatial operators. Although these schemes possess energy preserving properties, their convergence accuracy is limited to second order in time, especially for non-linear PDEs. The quest for a staggered and explicit time integration scheme that achieves fourth and sixth order temporal accuracy has motivated the current work, and prompted the investigation of the composition methods with the mimetic operators.

The composition methods are a staggered explicit temporal scheme based on recursive calculations at each step size, and have been investigated to solve the wave equation in, for example, [?]. These schemes exist up to sixth order accuracy [?], and have been noted to possess energy preserving qualities when applied to Hamiltonian systems [?]. In the current work, the high order composition schemes are investigated with the staggered high order Corbino-Castillo [?] mimetic operators to obtain energy preserving discretizations of the linear and non-linear Hamiltonian PDEs. The convergence properties of the proposed schemes are presented to illustrate our findings. The schemes achieve fourth and sixth order global spatio-temporal accuracy while preserving the numerical energy when applied to linear and non-linear Hamiltonian systems.

This paper is organized as follows: in section two, we outline the continuum wave equation and its Hamiltonian structure, and show the use of the extended Gauss divergence theorem to demonstrate the energy-stability of the system. In section three, we outline the mimetic methods and its formulation based on the extended Gauss divergence theorem. Section four presents the discrete version of the continuum problem, and demonstrates the applicability of the mimetic methods in discretely conserving the Hamiltonian function. The high order composition schemes are outlined in section five. Numerical results illustrating our findings are shown in section six, followed by concluding remarks.

2. The Continuous Problem

We consider the non-linear wave equation with homogeneous boundary conditions

$$\frac{\partial^2 u(x,t)}{\partial t^2} = \nabla \cdot \mathbb{K} \nabla u(x,t) - f'(u(x,t)), \quad \text{in } \Omega \times [0,T], (1)$$

subject to the initial and boundary conditions

$$u(x,0) = u_0(x), \quad \frac{\partial u}{\partial t}(x,0) = v_0(x) \quad \text{in } \Omega,$$
 (2)

$$u(x,t) = 0$$
 on $\partial\Omega \times [0,T]$ (3)

The domain $\Omega \in \mathbb{R}^d$ is a bounded region over the surface $\partial\Omega$, with the function f(u(x,t)) as a continuously differentiable real mapping $f: \mathbb{R} \to \mathbb{R}$ in a d-dimensional space. The quantity $\mathbb{K} \in \mathbb{R}^{d \times d}$ is a symmetric positive definite tensor. Some examples of non-linear equations that assume this form shown above are the sine-Gordon equation [?],

$$\frac{\partial^2 u(x,t)}{\partial t^2} = \nabla \cdot \mathbb{K} \nabla u(x,t) - \sin(u(x,t)) \tag{4}$$

and the non-linear improved Boussinesq equation [?],

$$\frac{\partial^2 u(x,t)}{\partial t^2} = \nabla \cdot \nabla u(x,t) + \frac{\partial^2}{\partial t^2} \nabla \cdot \nabla u + \nabla \cdot \nabla (u^2)$$
 (5)

An equivalent formulation for (1)-(2) as two first-order in time systems is given by

$$\begin{aligned} u_t(x,t) &= v(x,t) &&\text{in } \Omega \times [0,T], \\ v_t(x,t) &= \nabla \cdot \mathbb{K} \nabla u(x,t) - f'(u(x,t)) &&\text{in } \Omega \times [0,T], \end{aligned}$$

where the subscript $_t$ refers to the time-derivative. The initial and boundary conditions are given by

$$u(x,0) = u_0(x), \quad v(x,0) = v_0(x) \quad \text{in } \Omega,$$
 (8)

$$u(x,t) = 0,$$
 $v(x,t) = 0$ on $\partial \Omega \times [0,T]$ (9)

A well-known property of (1)-(2) is the conservation of energy, also referred to as the Hamiltonian function. The Hamiltonian function [?] is given by

$$\mathcal{H}(u,v,t) = \frac{1}{2} \int_{\Omega} \left(v^2 + \mathbb{K}(\nabla u)^2 + 2f(u) \right) dx \qquad (10)$$

The temporal evolution rate of the Hamiltonian function is evaluated as follows:

$$\frac{\partial \mathcal{H}}{\partial t} = \int_{\Omega} \left(vv_t + \nabla u \cdot \mathbb{K} \nabla v + f'(u) \right) dx$$
$$= \int_{\Omega} \left(v\nabla \cdot \mathbb{K} \nabla u + \nabla u \cdot \mathbb{K} \nabla v \right) dx$$
$$= \int_{\partial \Omega} v \cdot \mathbb{K} \nabla u \, dx$$
$$= 0$$

The conversion of the volume to surface integral in step three above arises from the use of the extended Gauss divergence theorem. Then, by incorporating the boundary conditions of (9), the evolution of the Hamiltonian is obtained to be constant with time. A key component here is the use of the extended Gauss divergence theorem. Spatial schemes that mimic this continuum property are an important necessity for energy preserving discretizations of Hamiltonian systems.

3. Mimetic Methods

Mimetic difference methods are based on constructing discrete differential operators that mirror their analog equivalents for conserved physical identities. These mimetic operators replicate the desired behavior found in their continuum counterparts. The resulting numerical solutions for PDEs obtained using mimetic methods are therefore expected to produce results that are physically more meaningful. The high order Castillo & Grone [?] mimetic operators are constructed to produce discrete differential operators that mimic the fundamental vector calculus quantities of divergence and gradient. These operators are incorporated on a staggered grid and achieve even orders of accuracy at the boundaries and interiors of a spatial grid. The resulting mimetic operators satisfy a discrete equivalent of the extended Gauss' divergence theorem, which is a global conservation law. The high order operators of Corbino & Castillo [?] have been shown to possess optimal bandwidth for the matrices. and eliminate the need for free-parameters for the discrete operators.

The idea behind mimetic methods is to construct operators that approximate the vector calculus identities of divergence and gradient. The extended Gauss' divergence theorem in a continuous domain $\Omega \subset \mathbb{R}^3$ of volume V enclosing the surface S is given by

$$\iiint_{\Omega} f \nabla \cdot \vec{v} \, dV + \iiint_{\Omega} \vec{v} \cdot (\nabla f) \, dV = \oiint_{\partial \Omega} f \vec{v} \cdot \vec{n} \, dS$$
 (11)

The resulting discrete mimetic operators **D** and **G** mimic the properties of their continuum counterparts $\nabla \cdot$ for divergence and ∇ for gradient. Here, \vec{n} is the outward normal to the boundary, and f and \vec{v} are smooth scalar and vector functions respectively. $\nabla \cdot$ is the divergence operator div, and ∇ the gradient operator grad. In the one dimensional domain $x \in [0, 1]$, this becomes integration by parts,

$$\int_0^1 f \frac{\mathrm{d}v}{\mathrm{d}x} \, \mathrm{d}x + \int_0^1 \frac{\mathrm{d}f}{\mathrm{d}x} v \, \mathrm{d}x = v \cdot f \Big|_0^1,\tag{12}$$

where $\frac{\mathrm{d}v}{\mathrm{d}x}$ and $\frac{\mathrm{d}f}{\mathrm{d}x}$ are the one-dimensional derivatives that correspond to the div and grad operators respectively. By setting either $f \equiv 1$ or $v \equiv 1$, the following conservation laws are obtained:

$$\int_0^1 \frac{\mathrm{d}v}{\mathrm{d}x} \, \mathrm{d}x = v \bigg|_0^1, \qquad \int_0^1 \frac{\mathrm{d}f}{\mathrm{d}x} \, \mathrm{d}x = f \bigg|_0^1 \tag{13}$$

The conservation laws noted above ensure the conversion between the integral within a domain to the integral over the surface.

Consider the functionals f and g in the functional space Ω endowed with the scalar property $\int_{\Omega} f \ g \ \mathrm{d}V \equiv \langle f,g \rangle_Q = f^\top Q g$ for some quadrature Q. The vector fields \vec{u} and \vec{v} are endowed with the vector property $\int_{\Omega} \vec{u} \ \vec{v} \ \mathrm{d}V \equiv \langle \vec{u}, \vec{v} \rangle_P = \vec{u}^\top P \vec{v}$ for some quadrature P. The Castillo-Grone

and Corbino-Castillo methods obtain high-order div and grad discretizations $\bf D$ and $\bf G$ that satisfy the order conditions

$$\frac{\mathrm{d}v}{\mathrm{d}x} \equiv \mathbf{D}\mathbf{v} + \mathcal{O}(\Delta h^k), \qquad \frac{\mathrm{d}f}{\mathrm{d}x} \equiv \mathbf{G}\mathbf{f} + \mathcal{O}(\Delta h^k) \quad (14)$$

Using the boundary operator \mathbf{B} , the discrete equivalent of (13) in the mimetic framework becomes

$$\langle \mathbf{D}\mathbf{v}, \mathbb{1} \rangle_{\mathcal{O}} = \langle \mathbf{B}\mathbf{v}, \mathbb{1} \rangle, \quad \langle \mathbf{G}\mathbf{f}, \mathbb{1} \rangle_{\mathcal{P}} = \langle \mathbf{B}\mathbf{f}, \mathbb{1} \rangle$$
 (15)

A discrete version of the extended Gauss' divergence theorem is

$$\langle \mathbf{D}\mathbf{v}, \mathbf{f} \rangle_{O} + \langle \mathbf{v}, \mathbf{G}\mathbf{f} \rangle_{P} = \langle \mathbf{B}\mathbf{v}, \mathbf{f} \rangle$$
 (16)

B is the boundary operator matrix that is comprised of zeros, with the top-left and bottom-right elements being -1 and 1. The system of algebraic equations in (15) is then solved individually to obtain the mimetic div and grad operators. The resulting div and grad operators do not exactly satisfy (16), but satisfy (16) up to an error term of order Δh [?]. The resulting mimetic boundary operator is denoted as $\hat{\bf B}$ and is obtained from

$$Q\mathbf{D} + \mathbf{G}^{\mathsf{T}} P = \hat{\mathbf{B}} \tag{17}$$

The boundary operator $\hat{\mathbf{B}}$ is comprised predominantly of zeros, with non-zero terms in the rows corresponding to the boundaries. While $\hat{\mathbf{B}}$ does not satisfy the mimetic constraint in (16) exactly, it has been demonstrated that $\hat{\mathbf{B}}$ converges to \mathbf{B} as $\Delta h \to 0$ [??]. A consequence of this observation is that when the discrete vectors \mathbf{v} are identical to zero at the boundaries (i.e., the term on the right-hand side of (11) is identical to zero), the duality relation $Q\mathbf{D} = -\mathbf{G}^{\mathsf{T}}P$ holds at the interiors of the grid. The duality relation also holds in the case of periodic boundary conditions. The mimetic operators therefore contribute to discretely mirroring the properties of the extended Gauss' divergence theorem by construction. Extensions of the mimetic operators to higher dimensions is obtained using Kronecker products [?].

4. The Semi-Discrete Problem

Consider a staggered one dimensional grid $X \in [0,1]$ discretized into N spatial elements of grid size $\Delta h = 1/N$. The divergence operator $\mathbf{D}: \mathcal{N} \to \mathcal{C}$ is defined at the cell centers, and is a mapping that operates on vectors $\begin{bmatrix} \mathbf{v}_0, \mathbf{v}_1, \dots, \mathbf{v}_N \end{bmatrix}^\mathsf{T}$ defined at the nodes. The gradient operator $\mathbf{G}: \mathcal{C} \to \mathcal{N}$ is defined at the nodes, and is a linear mapping that operates on scalars $\begin{bmatrix} \mathbf{f}_0, \mathbf{f}_{\frac{1}{2}}, \mathbf{f}_{\frac{3}{2}}, \dots, \mathbf{f}_{N-\frac{1}{2}}, \mathbf{f}_N \end{bmatrix}^\mathsf{T}$ defined at the cell-centers and boundaries. Using these mimetic high order operators, the continuous problem (6) is discretized as follows:

$$\mathbf{U}_t(X,t) = \mathbf{V}(X,t) \quad t \in [0,T]$$
(18)

$$\mathbf{V}_{t}(X,t) = \mathbf{D} \mathbb{K} \mathbf{G} \mathbf{U}(X,t) - \mathbf{F}'(\mathbf{U}(X,t))$$
 (19)

$$\mathbf{U}(X,0) = \mathbf{U}_0, \mathbf{V}(X,0) = \mathbf{V}_0 \tag{20}$$

The discretized Hamiltonian function is given by

$$\mathbf{H}[\mathbf{U}, \mathbf{V}] = \frac{1}{2} \left[\langle \mathbf{V}, \mathbf{V} \rangle_{Q} + \mathbb{K} \langle \mathbf{G} \mathbf{U}, \mathbf{G} \mathbf{U} \rangle_{P} + 2 \langle \mathbf{F}'(\mathbf{U}), \mathbb{1} \rangle \right]$$
(21)

The temporal evolution of the Hamiltonian function is

$$\frac{\partial \mathbf{H}}{\partial t} = \langle \mathbf{V}, \mathbf{D} \mathbb{K} \mathbf{G} \mathbf{U} \rangle_{Q} + \langle \mathbb{K} \mathbf{G} \mathbf{U}, \mathbf{G} \mathbf{V} \rangle_{P}$$
$$= \langle \mathbf{B} \mathbf{V}, \mathbb{K} \mathbf{G} \mathbf{U} \rangle$$
$$= 0$$

The semi-discrete mimetic representation of the wave equation preserves the Hamiltonian evolution over time, thereby mirroring the properties of its continuum case. The spatial discretization obtained using the high order Corbino-Castillo mimetic methods can therefore be considered as a valuable scheme for solving Hamiltonian systems.

5. Composition Schemes

Following the semi-discretization of the problem in the spatial domain, we now lay the framework for temporal integration schemes that preserve the intrinsic geometric properties of the PDE. The Hamiltonian system presented in the prior section can be represented as

$$\frac{\partial u}{\partial t} = \nabla_v \mathcal{H}, \quad \frac{\partial v}{\partial t} = -\nabla_u \mathcal{H}, \tag{22}$$

where ∇_u and ∇_v are gradients with respect to u and v. By introducing the symplectic matrix $\mathcal{J} = \begin{pmatrix} 0 & I \\ -I & 0 \end{pmatrix}$, we obtain

$$\begin{pmatrix} u_t \\ v_t \end{pmatrix} = \mathcal{J} \nabla_{uv} \mathcal{H}(u, v), \tag{23}$$

A property of Hamiltonian systems is the area (and volume) preservation, where the energy evolution of $\mathcal{H}(t)$ is a constant for all times t [?]: $\mathcal{H}(t) = \mathcal{H}(0) = \text{constant} \ \forall \ t \geq 0$. Moreover, the phase-pair evolution over time $(u(0), v(0)) \rightarrow (u(\tau), v(\tau))$ is a canonical transformation that preserves the symplectic 2-form wedge product $dp \land dq$ (where $dp \land dq(\xi_1, \xi_2) = dp(\xi_1) \ dq(\xi_2) - dp(\xi_2) \ dq(\xi_1)$) [?]. Temporal integration schemes that numerically preserve this intrinsic geometric property of Hamiltonian systems are said to be symplectic. The semi-discrete Hamiltonian formulation using the high order mimetic operators is denoted by

$$Q^{-1} \nabla_{\mathbf{v}} \mathbf{H}(\mathbf{u}, \mathbf{v}) = Q^{-1} Q \mathbf{v} = \mathbf{v}$$
 (24)

$$Q^{-1} \nabla_{\mathbf{u}} \mathbf{H}(\mathbf{u}, \mathbf{v}) = Q^{-1} \mathbf{G}^{T} P \mathbb{K} \mathbf{G} \mathbf{u}$$
 (25)

$$= -O^{-1}O\mathbf{D}\mathbb{K}\mathbf{G}\mathbf{u} = -\mathbf{D}\mathbb{K}\mathbf{G}\mathbf{u} \qquad (26)$$

The equality in (26) is a direct consequence of the duality relationship established in the prior section with the mimetic operators. The semi-discrete Hamiltonian system becomes

$$\begin{pmatrix} \mathbf{u}_t \\ \mathbf{v}_t \end{pmatrix} = \mathcal{J}Q^{-1} \ \nabla_{uv} \mathbf{H}(\mathbf{u}, \mathbf{v}), \tag{27}$$

where \mathcal{J} is the symplectic matrix and ∇_{uv} denotes the gradient with respect to the variables **u** and **v**.

Composition schemes stem from the fact that two halfsteps in time result in structure preserving discretizations that retain the symplectic nature of the PDE. The leapfrog scheme, or the schemes of Yee [?] are a classical example of a second order staggered temporal scheme. The s-stage composition method for the initial value problem $\mathbf{y}_t = \mathbf{f}(t, \mathbf{y}), \mathbf{y}(0) = \mathbf{y}_0$ is given by [??]

$$\boldsymbol{\psi}_{\mathbf{f},\Delta t} = \boldsymbol{\phi}_{\mathbf{f},\alpha_s\Delta t}^{(1)} \circ \boldsymbol{\phi}_{\mathbf{f},\beta_s\Delta t}^{(1*)} \circ \cdots \circ \boldsymbol{\phi}_{\mathbf{f},\alpha_1\Delta t}^{(s)} \circ \boldsymbol{\phi}_{\mathbf{f},\beta_1\Delta t}^{(s*)}, (28)$$

where each $\phi_{\mathbf{f},\alpha_i\Delta t}^{(i)}$, $\phi_{\mathbf{f},\beta_i\Delta t}^{(i*)}$ is a basic integration method for \mathbf{f} with temporal step $\alpha_i\Delta t$ or $\beta_i\Delta t$, α_i , β_i , $\Delta h\in\mathbb{R}$. We refer to [?] for the coefficients for the fourth and sixth order composition schemes. The recursive time-stepping scheme for the semi-discrete problem is as follows [??]:

$$\mathbf{u}_{k} - \mathbf{u}_{k-1} = -(\beta_{k} + \alpha_{k-1}) \Delta t \, \mathbf{v}_{k-1}$$

$$\mathbf{v}_{k} - \mathbf{v}_{k-1} = (\beta_{k} + \alpha_{k}) \Delta t \, \mathbf{D} \mathbb{K} \mathbf{G} \mathbf{u}_{k}, \quad k = 1, \dots, s$$

$$(29)$$

followed by the final step update

$$\mathbf{u}^{n+1} - \mathbf{u}_s = -\alpha_s \, \Delta t \, \mathbf{v}_s, \quad \mathbf{v}^{n+1} = \mathbf{v}_s \tag{30}$$

The fourth and sixth order composition schemes are investigated in the current work. The results are also compared with the fourth order Runge Kutta scheme, which is a non-symplectic scheme.

6. Numerical Results

Numerical examples that illustrate the proposed high order schemes are presented in this section. Where available, the analytical solution has been used to compare the numerical error with the discretized solution, and in obtaining a numerical order of convergence. The error between the analytical solution u and numerical solution u is evaluated using the infinity-norm, defined by

$$en = ||u(t^n) - \mathbf{U}(t^n)||_{\mathfrak{m}} \tag{31}$$

The numerical order of convergence q is calculated for each halving of step-size using

$$q = \frac{1}{\ln(2)} \frac{e n_{\Delta h}}{e n_{\Delta h/2}} \tag{32}$$

The following legends have been used in the tables and plots presented in this section: the fourth and sixth order mimetic operators are denoted by MIM4 & MIM6. The Runge Kutta (shown in each numerical example below for comparison to the composition schemes), fourth order and sixth order composition schemes are denoted by RK4, COMP4 and COMP6. The open-source library MOLE (Mimetic Operators Library Enhanced) [? ?] has been used for the Matlab implementation.

Table 1Order of accuracy, one-dimensional wave equation

m	$\Delta h = \Delta t$	MIM4-RK4		MIM4-COMP4		MIM6-COMP6	
		en	q	en	q	en	q
64	0.4688	0.2301		0.2194		0.1472	
128	0.2344	0.0681	1.756	0.0631	1.797	0.0103	3.842
256	0.1172	0.0060	3.512	0.0047	3.755	1.5974e-04	6.004
512	0.0586	4.3737e-04	3.770	3.4011e-04	3.780	3.3653e-06	5.568
1024	0.0293	2.7853e-05	3.972	2.1550e-05	3.980	5.7981e-08	5.859
2048	0.0146	1.7478e-06	3.994	1.3495e-06	3.997	9.2724e-10	5.966

Example 1. The wave equation (1) is solved in the one-dimensional domain $x \in [-15, 15]$, $t \in [0, T_e]$ with Dirichlet boundary conditions and initial condition given by

$$u(x,0) = \eta_{\mu,\sigma}(x) = e^{-1/\sigma^2} \left(x - \frac{\mu}{2} \right)^2, \sigma = 0.5, \mu = 0$$
 (33)

The analytical solution at time t is given by

$$u(x,t) = \eta_{u,\sigma}(x-t) \tag{34}$$

The order of convergence of the schemes is studied by integrating the system of equations until $T_e=1\ s$. The exact and numerical solutions are compared at T_e for each halving of the spatial size, and the order of convergence is calculated using the computed errors. Table 1 shows the computed errors and the orders of convergence with a CFL-condition of 1.0 (i.e., $\Delta h=\Delta t$). It can be noted that the schemes converge to fourth and sixth order accuracy as expected.

Figures 1, 2 show the numerical solution obtained using each of the schemes, at $T_e = 12 \text{ s}$. The fourth order schemes introduce oscillations at the leading edge of the impulse function, while the sixth order scheme produces a result that more closely resembles that of the analytical solution.

Figure 3 shows the energy evolution of the one-dimensional wave equation, normalized to the energy at t=0. The Runge Kutta scheme shows a decaying energy over time, while the fourth and sixth order mimetic composition schemes conserve the numerical energy.

Example 2. The convergence and energy evolution in twoand three-dimensional spaces for the wave equation is presented in this example. In two-dimensions, the domain is defined as $(x, y) \in [-15, 15]^2$ with initial condition u(x, y) = $\eta_{\mu,\sigma}(x) + \eta_{\mu,\sigma}(y)$. The analytic solution is given by u(x, y, t) = $\eta_{\mu,\sigma}(x-t) + \eta_{\mu,\sigma}(y-t)$.

In three-dimensional space $(x, y, z) \in [-25, 25]^3$, the initial condition is specified as $u(x, y, z) = \eta_{\mu,\sigma}(x) + \eta_{\mu,\sigma}(y) + \eta_{\mu,\sigma}(z)$, with analytic solution given by $u(x, y, z, t) = \eta_{\mu,\sigma}(x-t) + \eta_{\mu,\sigma}(y-t) + \eta_{\mu,\sigma}(z-t)$.

Convergence is evaluated by comparing the analytic and numerical solutions at time $T_e=1$ s. The convergence properties of the two-dimensional wave equation is shown in table 2, with a CFL condition of $\frac{\Delta t}{\Delta h}=0.5$, step sizes along the x and y directions denoted by $\Delta h_x=\Delta h_y=\Delta h$. In table

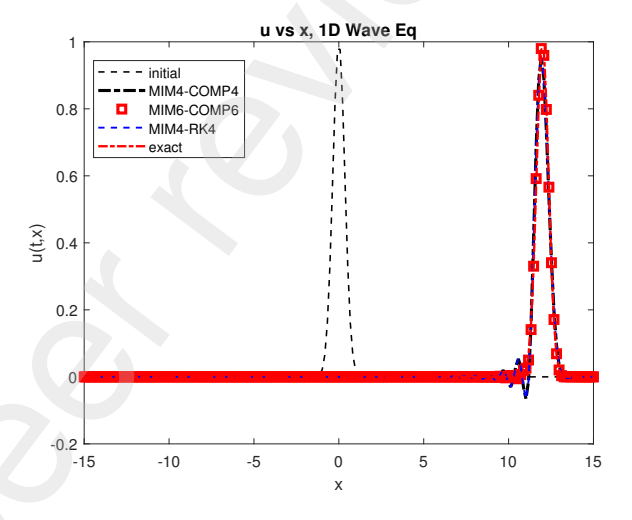


Figure 1: Numerical Solution, one-dimensional wave equation

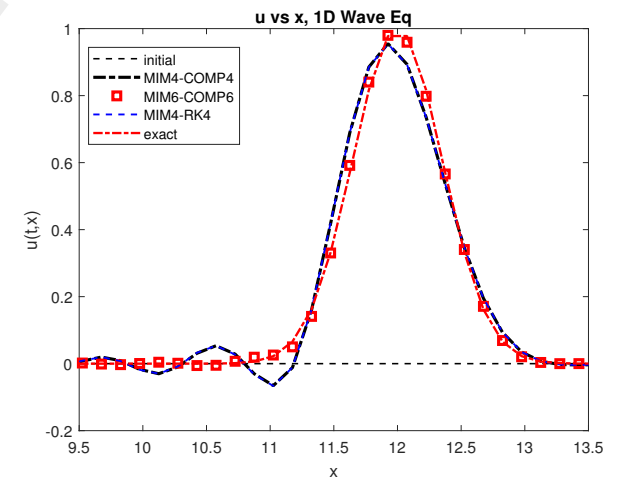


Figure 2: Numerical Solution, one-dimensional wave equation, zoomed-in

3, the convergence properties are shown for a fixed timestep $\Delta t = 0.01 \, s$, and the spatial step-size halved for each simulation. In both instances, the desired order of accuracy is attained for the fourth and sixth order schemes.

The energy evolution of the two- and three-dimensional wave equation is shown in figures 4, 5. The high order

Table 2 Order of accuracy, two-dimensional wave equation with fixed CFL, $\Delta h = 2\Delta t$

m	Δh	MIM4-RK4		MIM4-COMP4		MIM6-COMP6	
=n	$=2\Delta t$	en	q	en	q	en	q
128	0.2344	0.0924		0.0895		0.0341	
256	0.1172	0.0092	3.333	0.0086	3.377	9.6709e-04	5.138
512	0.0586	6.1004e-04	3.908	5.7507e-04	3.904	1.7857e-05	5.759
1024	0.0293	3.8763e-05	3.976	3.6565e-05	3.975	2.9358e-07	5.926

Table 3 Order of accuracy, two-dimensional wave equation with fixed $\Delta t = 0.01 \text{ s}$

m	Δh	MIM4-RK4		MIM4-CO	MP4	MIM6-CO	MIM6-COMP6	
=n		en	q	en	q	en	q	
128	0.2344	0.0817		0.0817		0.0330		
256	0.1172	0.0087	3.239	0.0087	3.239	0.0010	4.996	
512	0.0586	5.7464e-04	3.912	5.7418e-04	3.913	1.9298e-05	5.742	
1024	0.0293	3.6806e-05	3.964	3.6329e-05	3.982	3.1110e-07	5.955	

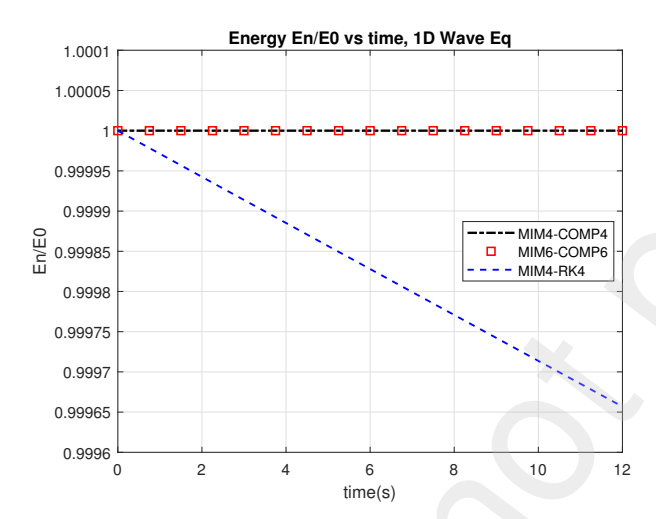


Figure 3: Energy Evolution, one-dimensional wave equation

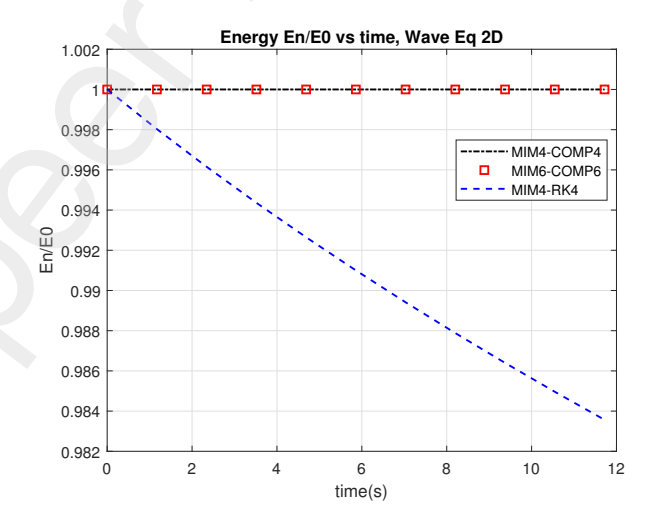


Figure 4: Energy Evolution, two-dimensional wave equation

mimetic-composition schemes preserve the Hamiltonian function over time, and thereby leading to superior numeric properties when applied to Hamiltonian PDEs.

Example 3. The sine-Gordon equation is presented in this example. We start with the one-dimensional case, where the forcing function in (1) is given by f'(u) = sin(u). The initial condition is given by [?]

$$u(x,0) = 4\arctan\left(e^{\lambda}\right),\tag{35}$$

$$u(x,0) = 4 \arctan(e^{\lambda}),$$
 (35)
 $v(x,0) = -\frac{4ce^{\lambda}}{\sqrt{1-c^2}(1+e^{2\lambda})}, \quad \lambda = \frac{x-ct}{\sqrt{1-c^2}}$ (36)

and the analytical solution given by

$$u(x,t) = 4\arctan\left(e^{x-ct/\sqrt{1-c^2}}\right)$$
(37)

The conserved quantity for the sine-Gordon equation is the Hamiltonian function

$$\mathcal{H}(u,t) = \frac{1}{2} \int_{\Omega} \left(v^2 + \mathbb{K}(\nabla u)^2 + 2(1 - \cos u) \right) dx$$
 (38)

The problem is defined in the domain $x \in [-50, 50]$ with c =0.5 and periodic boundaries. The numerical solution and the order of convergence for the schemes is shown in figures 6, 7. Convergence was evaluated with a CFL condition of 0.25. In addition to achieving the desired order of convergence, the high order mimetic-composition schemes display energy conserving properties as shown in figure 8. In contrast, the Runge Kutta scheme shows an asymptotically increasing energy over time.

The energy evolution and the numerical solution for the two-dimensional sine-Gordon equation is depicted in figures 9, 11. The two-dimensional domain is $(x, y) \in [-50, 50]^2$

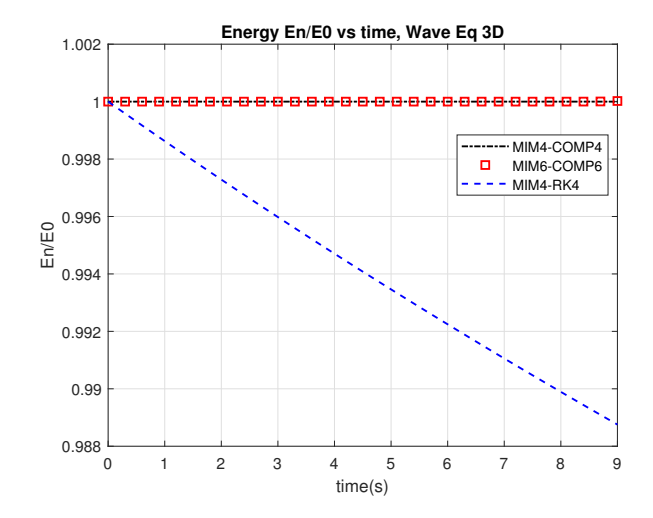


Figure 5: Energy Evolution, three-dimensional wave equation

with periodic boundaries. The initial condition is taken from the two-dimensional analytical solution of the form [??]

$$u(x, y, t = 0) = -4\arctan\left(\lambda_{xy}\right) \tag{39}$$

$$\lambda_{xy} = \frac{c}{\sqrt{1 - c^2}} \sin(0.5) \operatorname{sech}(cx) \operatorname{sech}(cy)$$
 (40)

with c = 0.5. The equations were integrated up to $T_{e} =$ 50 s. The three-dimensional case was solved using the initial condition

$$u(x, y, t = 0) = -4\arctan\left(\lambda_{xyz}\right)$$

$$\lambda_{xyz} = \frac{c}{\sqrt{1 - c^2}} \sin(0.5) \operatorname{sech}(cx) \operatorname{sech}(cy) \operatorname{sech}(cz)$$
(41)

(42)

with c = 0.5, in the domain $(x, y, z) \in [-50, 50]^3$, and integrated up to $T_e = 40 \text{ s}$. The energy evolution is shown in fig. 10. It can be observed that the numerical energy is conserved in one-, two- and three-dimensional cases for the sine-Gordon equation with the mimetic-composition schemes.

Example 4. In this example, we evaluate the Boussinesq equation [?] of the form

$$u_{tt} = \nabla \cdot \nabla (u_{tt}) + \nabla \cdot \nabla (u + u^2) \tag{43}$$

written as two first-order in time system of equations

$$u_t = v \tag{44}$$

$$u_t = v$$

$$(I - \nabla^2) v_t = \nabla^2 (u + u^2)$$

$$(45)$$

Here, ∇^2 is the Laplacian operator. The conserved quantity

$$\mathcal{H}(t) = \frac{1}{2} \int_{\Omega} \left(v^2 + (u_t)^2 + u^2 + \frac{2}{3} u^3 \right) dx \tag{46}$$

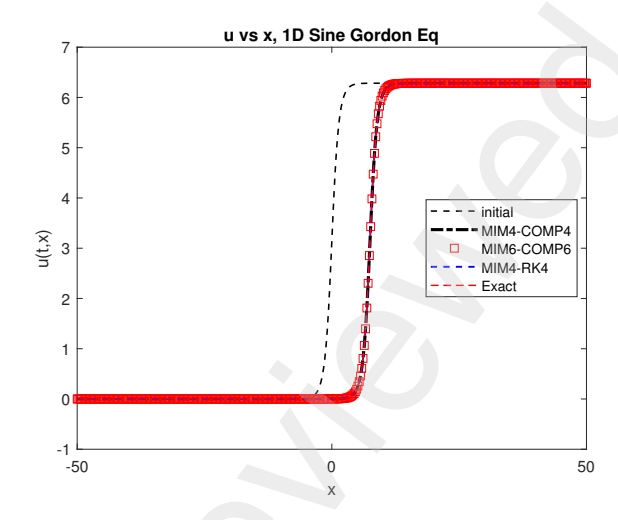


Figure 6: Numerical solution, one-dimensional sine-Gordon equation

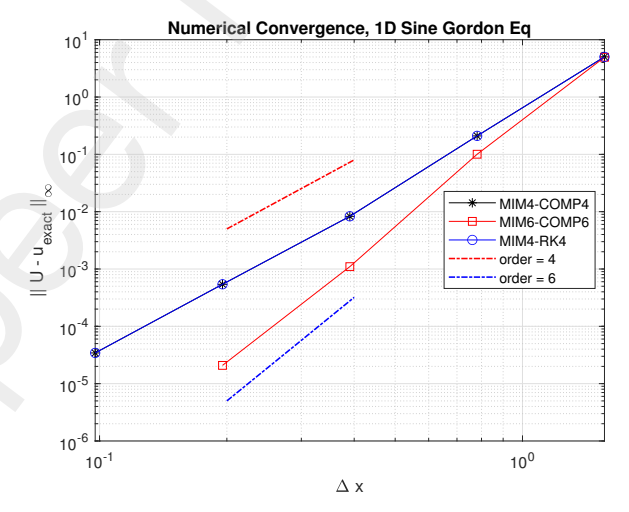


Figure 7: Numerical convergence, one-dimensional sine-Gordon equation

The initial conditions for the one-dimensionnal case are calculated using the known analytical solution

$$u(x,t) = \alpha \operatorname{sech}^{2}\left(\sqrt{\frac{\alpha}{6}} \frac{x - \beta t - x_{0}}{\beta}\right),$$

$$\alpha = 0.5, x_{0} = 0, \beta = \sqrt{1 + \frac{2\alpha}{3}}$$
(47)

The order of convergence and energy evolution of the numerical solution solved in the one-dimensional domain $x \in [-50, 50]$ is shown in figures 12, 13. The desired order of accuracy and energy conservation can be noted for the mimetic-composition schemes for this example as well.

Figure 14 shows the energy evolution of the Boussinesq equation in the two-dimensional domain $(x, y) \in [-60, 60]^2$ with initial conditions as shown in example 2. Energy conservation can be noted here for the mimetic-composition schemes, while the RK scheme exhibits an asymptotic

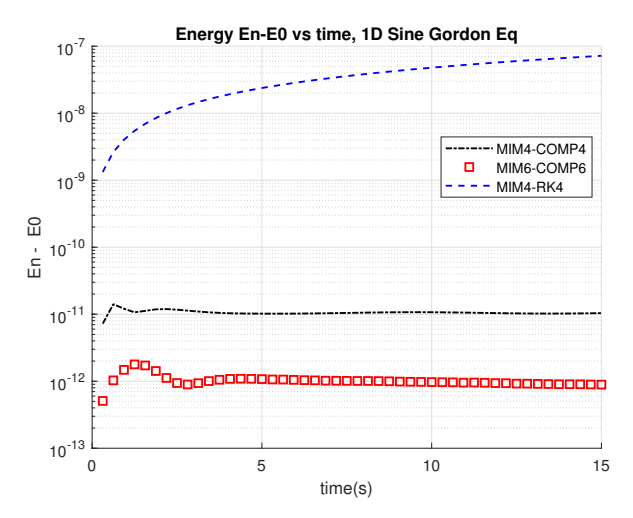


Figure 8: Energy evolution, one-dimensional sine-Gordon equa-

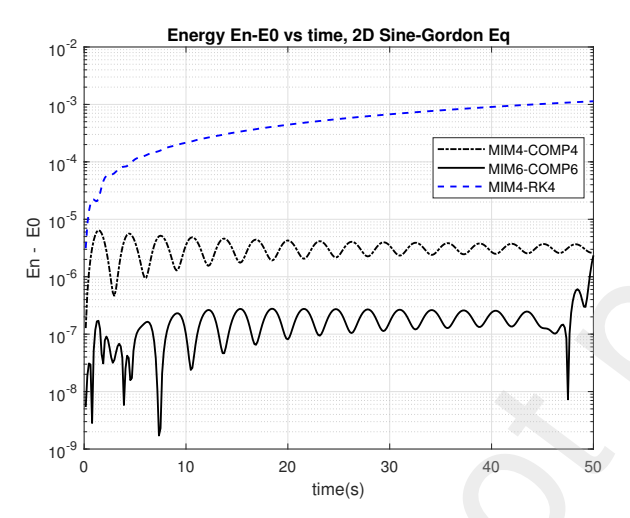


Figure 9: Energy evolution, two-dimensional sine-Gordon equation

divergence in the energy.

Example 5. The last example presented is the non-linear shallow water system of equations adapted from [?], given by

$$\eta_t + \nabla \cdot (u + \eta u) = 0 \tag{48}$$

$$u_t + \nabla \eta + u \nabla \cdot u = 0, \tag{49}$$

with the conserved Hamiltonian function $\mathcal{H}=\frac{1}{2}\int_{\Omega}u^2+\eta^2+\eta^2+\eta^2$ dx. The numerical solution was evaluated on a one-dimensional domain $x\in[-40,40]$, with initial conditions $u(x,0)=1+0.1\exp\left(-x^2\right),\ v(x,0)=0$, and periodic boundaries. The numerical solution evaluated using a spatial grid of 400 elements and a time-step size of 0.01 s at $T_e=15\ s$ is shown in figures 15, 16. The mimetic methods capture the non-linear behavior of the solution well, given that this equation is subject to a shock behavior.

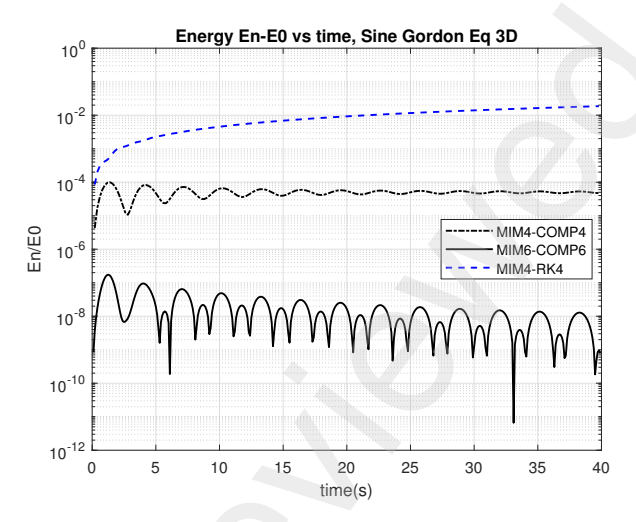


Figure 10: Energy evolution, three-dimensional sine-Gordon equation

The mimetic-composition schemes also show conservation of energy behavior, which is not reflected with the Runge Kutta method. A similar behavior can also be observed in figure 17 for the three-dimensional case solved in the domain $(x, y, z) \in [-25, 25]^3$ with the same initial condition as in example 2.

7. Conclusion

The high order mimetic methods produce mimetic vector calculus operators that mimic a conservation law. The resulting schemes for partial differential equations obtained using these operators stay faithful to the physics. In this work, the high order mimetic operators are used with the structure preserving composition temporal schemes for the numerical integration of Hamiltonian systems. The energy preserving nature of these numerical schemes is illustrated for Hamiltonian systems in this paper. Numerical examples that demonstrate the order of convergence for linear and non-linear problems in one-, two- and three-dimensions are presented. A novelty of the results presented in this paper is the sixth order energy preserving mimetic scheme for non-linear Hamiltonian systems. The high order mimeticcomposition schemes are therefore a valuable tool for the numerical solution of Hamiltonian systems.

Disclosure And Data Availability

The numerical results presented in this paper were performed on Matlab with the open source library MOLE, https://github.com/csrc-sdsu/mole. The Matlab scripts associated with these examples can be found in https://github.com/asrinivasan0709/HONOM2024. This work was funded by the Computational Science Research Center, San Diego State University.

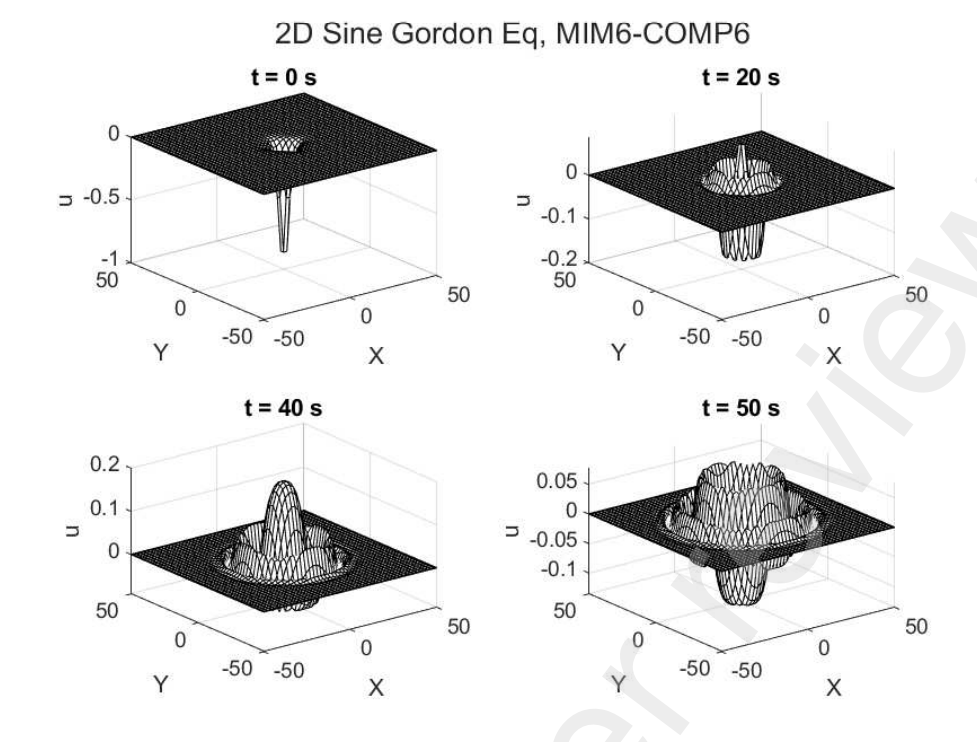


Figure 11: Numerical solution, two-dimensional sine-Gordon equation

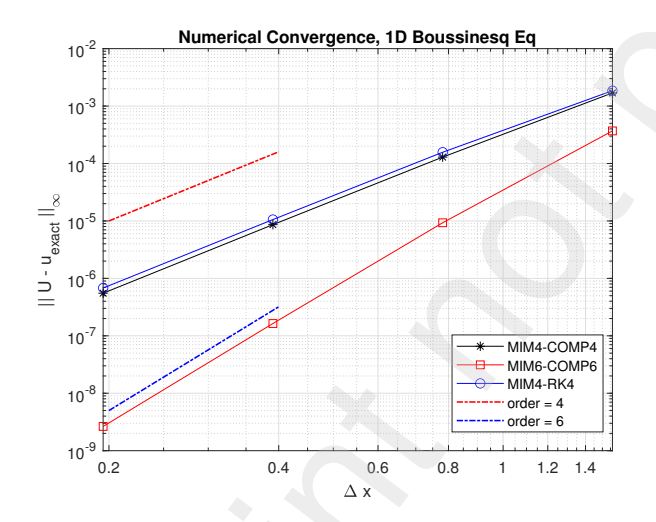


Figure 12: Convergence, one-dimensional Boussinesq equation

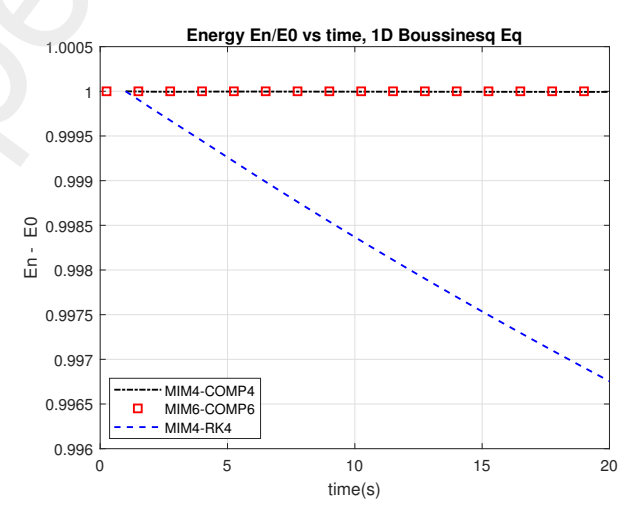


Figure 13: Energy evolution, one-dimensional Boussinesq equation

In memoriam

This paper is dedicated to the memory of Prof. Arturo Hidalgo López (*July 03rd 1966 - †August 26th 2024) of the Universidad Politecnica de Madrid, organizer of HONOM 2019 and active participant in many other editions of HONOM. Our thoughts and wishes go to his wife Lourdes and his sister María Jesús, whom he left behind.

CRediT authorship contribution statement

Anand Srinivasan: Conceptualization, Methodology, Validation, Writing. **José E. Castillo:** Methodology, Supervision, Reviewing, Editing.

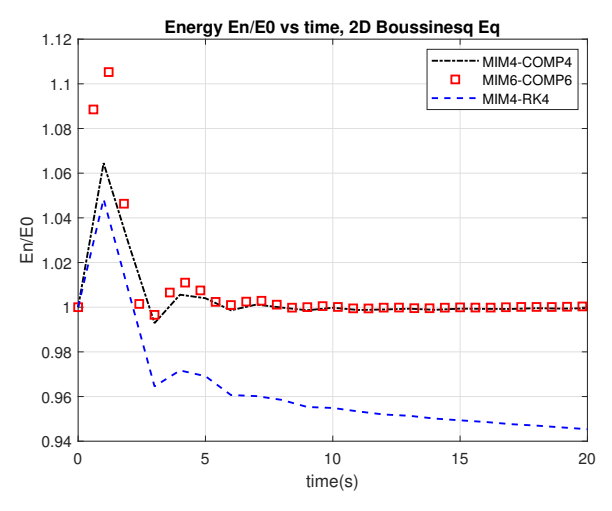


Figure 14: Numerical solution, two-dimensional Boussinesq equation

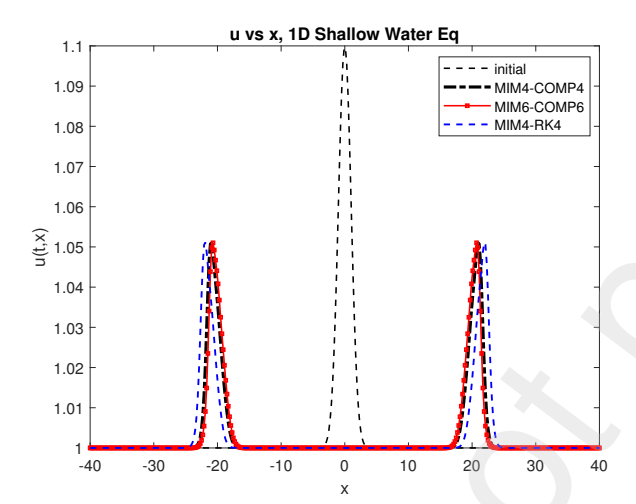


Figure 15: Numerical solution, one-dimensional shallow water equation

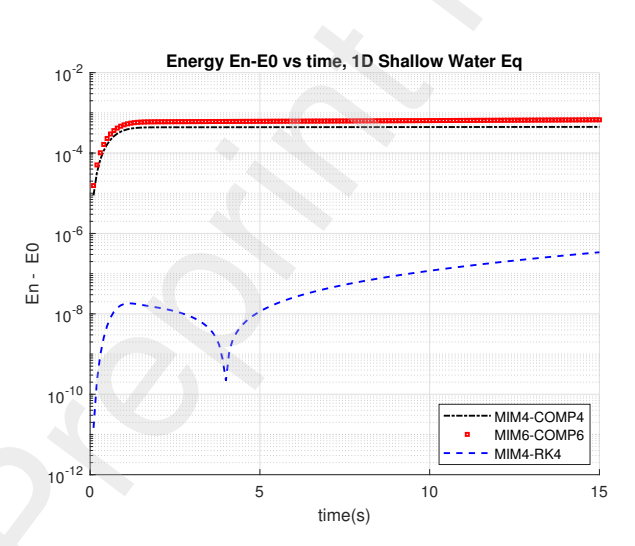


Figure 16: Energy evolution, one-dimensional shallow water equation

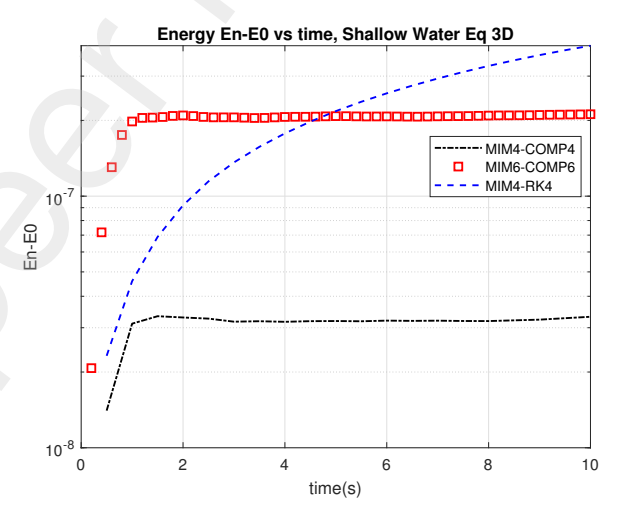


Figure 17: Energy evolution, 3D shallow water equation